Check for updates

APPLIED SCIENCES AND ENGINEERING

PhoCoil: A photodegradable and injectable single-component recombinant protein hydrogel for minimally invasive delivery and degradation

Nicole E. Gregorio[1], Fan Zhang[1], Yusuke Suita[2], Lisa S. Ang[2], Olivia Prado[1], Arafat Fasuyi[1], James M. Olson[2,3], Kelly R. Stevens[1,4,5], Cole A. DeForest[1,5,6,7,8,9]*

Copyright © 2025 The Authors, some rights reserved; exclusive licensee American Association for the Advancement of Science. No claim to original U.S. Government Works. Distributed under a Creative Commons Attribution NonCommercial License 4.0 (CC BY-NC).

Hydrogel biomaterials offer great promise for three-dimensional cell culture and therapeutic delivery. Despite many successes, challenges persist in that gels formed from natural proteins are only marginally tunable whereas those derived from synthetic polymers lack intrinsic bioinstructivity. Toward the creation of biomaterials with both excellent biocompatibility and customizability, recombinant protein–based hydrogels have emerged as molecularly defined and user-programmable platforms that mimic the proteinaceous nature of the extracellular matrix. Here, we introduce PhoCoil, a dynamically tunable recombinant hydrogel formed from a single protein component with unique multistimuli responsiveness. Physical cross-linking through coiled-coil interactions promotes rapid shear-thinning and self-healing behavior, rendering the gel injectable, whereas an included photodegradable motif affords on-demand network dissolution via visible light. PhoCoil gel photodegradation can be spatiotemporally and lithographically controlled in a dose-dependent manner, through complex tissue, and without harm to encapsulated cells. We anticipate that PhoCoil will further enable applications in tissue engineering and regenerative medicine.

INTRODUCTION

Hydrogels provide specialized material environments that are conducive to studying cells in three-dimensional (3D) as extracellular matrix mimics and delivering therapeutics in a controlled manner (*1*–*3*). However, many of the most popular hydrogels used in biological or biomedical applications suffer from either a lack of tunability or shortcomings in their biocompatibility or biodegradability. In the case of naturally derived materials consisting of biomolecules extracted from tissues, precise control over material properties remains elusive or requires additional synthetic modifications (*4*, *5*). Moreover, batch-to-batch variability in these natural materials can be an insurmountable hurdle to both experimental consistency and approval for clinical use (*6*, *7*). Although biomaterials research has also favored synthetic polymer–based materials for their ability to be readily modified and controlled by the user, these materials are infrequently chosen for therapeutic applications due to concerns of low cytocompatibility and biodegradability or high immunogenicity, as well as their intrinsic polydispersity (*5*, *7*, *8*). On top of this, these materials often require substantial expertise in synthetic chemistry to install the reactive and responsive chemical handles that enable user-specified network customization, rendering them unreachable by many biologically focused groups.

Over the past 25 years, recombinant protein–based hydrogels have become an enticing alternative to natural and synthetic polymer hydrogels. Recombinant protein hydrogels can bridge the gap—retaining both a highly biocompatible and bioresorbable makeup similar to natural protein–based gels while providing greater user-defined tunability without the need for synthetic chemistry (*5*, *7*, *8*). The ability to control the mechanical and responsive characteristics of these protein networks is genetically encoded, arising from user-defined variations at the amino acid and fusion protein levels, which can be readily modified through well-established cloning techniques already common across the biological sciences. Furthermore, recombinant protein production can be accomplished with relatively simple and widely used bacterial protein expression techniques and common laboratory equipment. Recombinant protein–based materials have the added benefit of being familiar substrates for cells; they can easily be designed to promote cell-material interactions through the inclusion of cell binding motifs and can be processed and broken down by preexisting cellular machinery (*5*, *8*). Collectively, these properties make recombinant protein hydrogels well suited toward biomedical applications such as localized therapeutic cell delivery.

In this work, we sought to design and characterize a recombinant biomaterial system with potential for minimally invasive cell delivery and user-controlled cell release. To achieve this, we envisioned a material that was both injectable and photodegradable while retaining high biocompatibility. Our group recently developed an injectable recombinant protein–based hydrogel that uses coil motifs as physically cross-linking domains linked together via an unstructured flexible linker called XTEN (*9*). The shear-thinning and self-healing nature of this telechelic, single-component hydrogel maintained high viability of encapsulated cells throughout and following injection both in vitro and in vivo. Although this physically cross-linked XTEN hydrogel slowly degrades through surface erosion, the timing of degradation is beyond user control.

Building on this work, we sought to introduce photodegradability to the material to enable user-actuated spatiotemporal control of network degradation. We anticipated that the insertion of a previously evolved protein called PhoCl (*10*) at the center of the XTEN

[1]Department of Bioengineering, University of Washington, Seattle, WA 98195, USA. [2]Seattle Children's Research Institute, Seattle, WA 98101, USA. [3]Department of Pharmacology, University of Washington, Seattle, WA 98195, USA. [4]Department of Laboratory Medicine & Pathology, University of Washington, Seattle, WA 98195, USA. [5]Institute for Stem Cell & Regenerative Medicine, University of Washington, Seattle, WA 98195, USA. [6]Department of Chemical Engineering, University of Washington, Seattle, WA 98195, USA. [7]Department of Chemistry, University of Washington, Seattle, WA 98195, USA. [8]Molecular Engineering & Sciences Institute, University of Washington, Seattle, WA 98195, USA. [9]Institute for Protein Design, University of Washington, Seattle, WA 98195, USA.
*Corresponding author. Email: profcole@uw.edu

Downloaded from https://www.science.org on September 06, 2025

linker would introduce this photodegradable response (Fig. 1). PhoCl is a photocleavable protein whose peptide backbone undergoes irreversible cleavage at the chromophore in response to 405-nm light, providing both a cytocompatible and highly bioorthogonal trigger for 4D control of protein cleavage (*10*–*12*). Previous works from our group and others have shown PhoCl's utility in introducing photoresponsivity to hydrogels (*13*–*16*). The resulting material, referred to as "PhoCoil," achieves the intended combination of chemical, physical, and stimuli-responsive properties (biocompatible, injectable, photodegradable), which are all directly specified in its molecular design. Our PhoCoil material offers unique benefits over previously reported photodegradable recombinant protein–based materials (*16*–*24*) as it is formed directly from a single protein component, requires no small molecules to initiate gelation and/or photocleavage, is stable under ambient light for easy handling, is readily injectable in its gel state, and degrades fully in response to cytocompatible visible light. In addition, our work is one of the few examples of a transdermally triggerable photoresponse from a hydrogel material (*25*–*29*). Here, we thoroughly characterize PhoCoil's physical and light-responsive properties as well as provide proof-of-concept studies highlighting its potential as an injectable cell delivery and triggered release platform.

RESULTS

Protein design

The PhoCoil protein represents a new design that builds on our team's prior efforts in the recombinant protein hydrogel space (*9*) by encoding photodegradability into the primary protein sequence. PhoCoil's design is similar to that of a symmetric pentablock copolymer containing three distinct segments arranged in an ABCBA pattern that each individually contributes to its macromolecular properties (Fig. 1). This telechelic protein has self-associating coil domains at both termini (Block A), allowing for network formation through physical interactions between individual protein units. These flanking coils are naturally derived from the cartilage oligomeric matrix protein sequence and form homopentameric bundles that associate through noncovalent interactions along the length of the coils (*30*, *31*). Because of these physical interactions, coil association is reversible under varying force. For example, high-strain conditions pull apart the coiled-coil structures, resulting in shear thinning of the network and a transition to a liquid-like state. Subsequent return to a low-strain state allows the coiled coils to reform, returning the network to its original, gel-like state. This shear-thinning and self-healing behavior of the network enables injection through small-gauge needles postgelation. We take advantage of coiled-coil domains as they have been widely used to create physically cross-linked protein biopolymer networks, enabling a variety of applications in injectable, sustained drug delivery (*8*, *32*–*39*).

At the center of the protein is PhoCl (Block C), a green fluorescent protein that undergoes irreversible cleavage in response to 405-nm light, providing the network with its photodegradable properties (*10*). PhoCl cleavage occurs in the chromophore of the protein, where visible light induces a β-elimination reaction that results in scission of the peptide backbone, producing a short-lived red state of the protein. This red state is temporarily captured in our hydrogels and dissipates as the two halves of the protein diffuse away from each other, resulting in the dissolution of the gel network as the coiled-coil bundles are no longer covalently linked. Given this cleavage mechanism, PhoCoil gels undergo rapid softening upon 405-nm light exposure, indicated by a color change in the material, followed by full degradation of the network. In this work, we used the recently evolved PhoCl2c variant to provide the most complete PhoCl cleavage possible, which we found essential to forming a truly photodegradable network (*40*).

Connecting the two coil domains to the central PhoCl protein is XTEN (Block B), a pseudo-repeat protein sequence containing only A, S, T, P, G, and E amino acids. XTEN was originally evolved as a protein mimic of PEG (polyethylene glycol) to "eXTENd" the circulating half-life of drugs in the body (*41*, *42*). As such, it was specifically

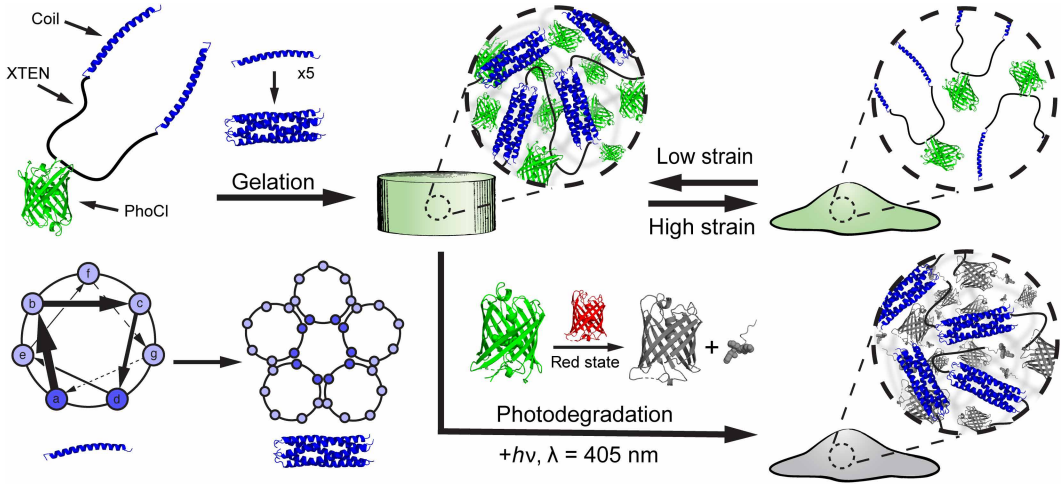

Fig. 1. PhoCoil structure and stimuli-responsive properties. PhoCoil hydrogels are physically self-assembled through homopentameric coiled-coil bundle formation. These bundles are held together by noncovalent interactions along the length of the helices, primarily between amino acids at the a and d positions. The noncovalent nature of these associations endows the bulk gel with shear-thinning and self-healing properties in response to applied force. The network degrades in response to 405-nm light due to the cleavage of the peptide backbone within the chromophore of PhoCl. During this process, PhoCl temporarily occupies a red state before the diffusive separation of the two protein halves and subsequent network disassociation. Protein Data Base ID Codes: PhoCl intact (green state), 7DMX; PhoCl cleaved (red state), 7DNA; PhoCl cleaved and dissociated (colorless state), 7DNB; coiled coil, 1MZ9.

Downloaded from https://www.science.org on September 06, 2025

designed to be high expressing and unstructured, with the restricted amino acid makeup chosen to minimize immunogenicity. In PhoCoil, we use a 144–amino acid variant of XTEN, split into two 72 amino acid segments by the PhoCl protein. XTEN provides flexibility to the PhoCoil protein, minimizing steric restrictions to further encourage intermolecular interactions. In this way, XTEN functions as an alternative to the widely used elastin-like protein (ELP) linkers seen in many recombinant protein hydrogel designs used for 3D cell culture and delivery (*6*, *19*, *32*–*36*, *43*–*47*).

Expression and purification of the PhoCoil protein yielded a solution that fluoresced green and contained protein of the expected molecular weight by mass spectroscopy (fig. S1). PhoCoil also displayed the expected photocleavage activity in solution via mass spectroscopy and sodium dodecyl sulfate–polyacrylamide gel electrophoresis (SDS-PAGE) analysis, with ~75% of the total protein cleaving in response to visible light (figs. S1 and S2). We hypothesize that the remaining 25% of intact PhoCoil observed in SDS-PAGE lacks a properly matured chromophore, inhibiting its ability to undergo the expected photocleavage. This hypothesis is supported by the disappearance of the mature, intact PhoCoil peak after 405-nm light exposure and concomitant appearance of an immature, intact PhoCoil peak indicated by a comparative +18-Da shift (*10*) (fig. S1).

Characterization of stiffness, shear thinning, and self-healing behavior

Mechanical characterization of PhoCoil gels was conducted via oscillatory shear rheology. At constant low strain (5%) and frequency (10 rad s^{-1}) within the linear viscoelastic range, we found that gel stiffness as measured by the storage modulus could easily be modulated between 1 and 4 kPa by varying the weight percent of the gel (7.5 to 12.5 wt %) (Fig. 2A). This allowed us to capture the mid-range of soft tissue stiffness in the body, which vary from 0.5 to 30 kPa (*48*). Frequency sweeps indicated no crossover within the tested range of 0.1 to 50 rad s^{-1} (Fig. 2B). Shear and strain sweeps demonstrated the shear-thinning behavior of the gel, with the viscosity decreasing by two orders of magnitude or more as the shear rate increased from 0.1 to 50 s^{-1} (Fig. 2C). Strain sweeps indicated a gel-sol transition, signified by a crossover in G' and G'', for all gel weight percentages. The 7.5 and 10 wt % gel-sol transitions occur around 50% strain, whereas the 12.5 wt % gel transition occurred at 150% strain (Fig. 2, D and E). These viscoelastic properties are typical of coiled coil–based protein hydrogels (*49*).

Cyclic strain sweeps were conducted to investigate the ability of PhoCoil gels to repeatedly shear-thin and self-heal via the self-associating coil domains. When the strain was increased from 5 to 500%, well above the strain crossover for all gels, G'' dominated, indicating that the gels were occupying a liquid-like state (Fig. 2F). This transition happened in under 2 s, the minimum sampling interval achievable for this test. When the material was returned to 5% strain, far below the strain crossover, it quickly returned to a gel state, where G' dominates. Upon this regelation, stiffnesses similar to the initial G' were achieved. All gel weight percentages were able to undergo repeated, rapid shear-thinning and complete self-healing over four high strain periods. These shear-thinning and self-healing

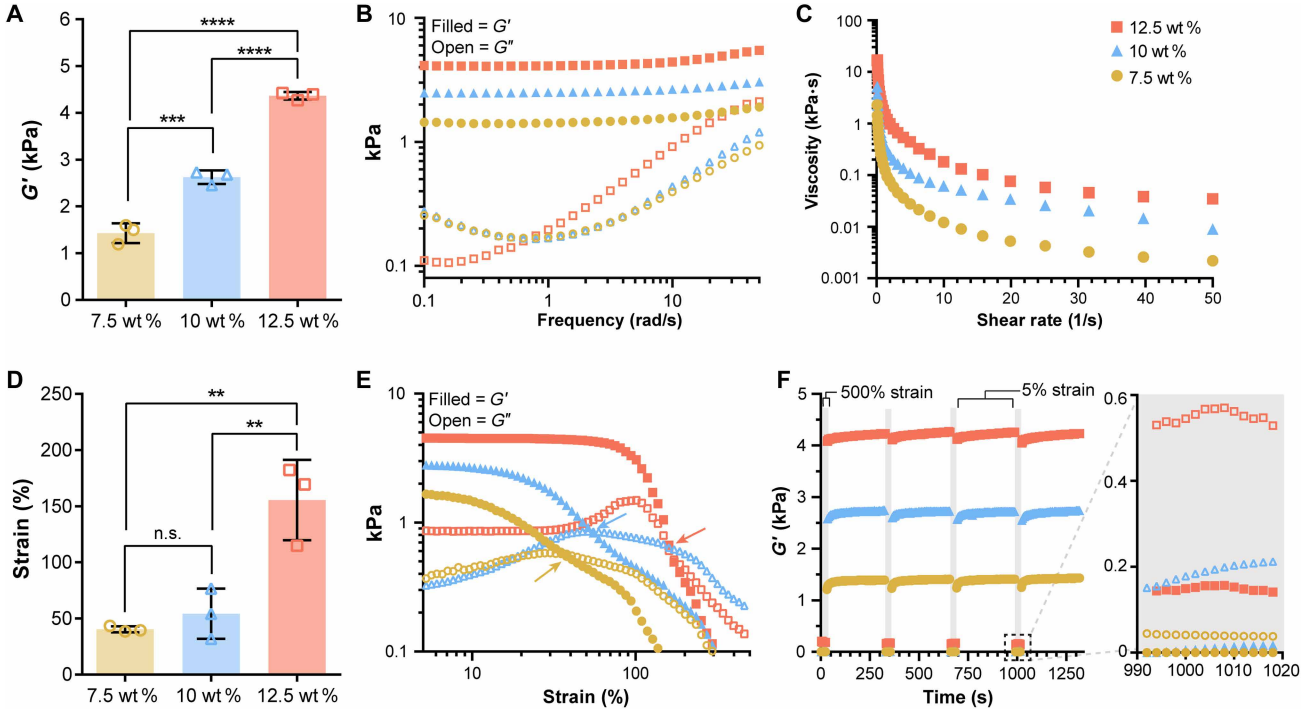

Fig. 2. Viscoelastic properties of PhoCoil gels. (**A**) G' determined from oscillatory rheology time sweeps at 25°C, 5% strain, 10 rad s^{-1} with varied gel weight percentage. (**B**) Representative frequency sweep test at 25°C with fixed 5% strain. (**C**) Representative viscosity profile during shear-sweep test at 25°C. (**D** and **E**) Strain-sweep test at 25°C with fixed 10 rad s^{-1} frequency. (D) Strain crossover value indicated by the arrows in each selected representative strain sweep shown in (E). (**F**) Cyclic strain sweep test at 25°C. The frequency was fixed at 10 rad s^{-1}, and the strain was held at 500% in gray regions (30 s) and 5% in white regions (600 s). A magnified view of one high strain interval is shown to demonstrate the strain induced gel-sol transition. For all graphs, filled symbols represent G', and open symbols represent G''. All bars represent the means ± SD of three independently formed gels for each weight percentage. Significance testing was performed using Tukey's multiple comparisons test. n.s., not significant; *$P < 0.05$, **$P < 0.01$, ***$P < 0.001$, ****$P < 0.0001$.

Downloaded from https://www.science.org on September 06, 2025

behaviors indicate that PhoCoil should be easily injectable postgelation (*2*, *50*). Injectability was confirmed by visualization of injection through a 25-gauge needle, where a stable gel is formed after exit from the needle (fig. S3 and movies S1 and S2).

Light-induced degradation and controlled softening

We next aimed to characterize PhoCoil's ability to soften and degrade in response to 405-nm light. To do so, we used a photorheometer setup that permits controlled light delivery to the gel while simultaneously measuring its mechanical properties. We found that PhoCoil gels at all weight percentages degrade in a similar "exponential decay" manner, with first-order rate constants of 0.0293 ± 0.0009 min^{-1} (7.5 wt %), 0.024 ± 0.002 min^{-1} (10 wt %), and 0.023 ± 0.002 min^{-1} (12.5 wt %), corresponding to half-lives of 23.7 ± 0.7 min, 29 ± 2 min, and 31 ± 3 min, respectively. All weight percentages showed a plateau stiffness that was consistently 20 to 30% of the initial stiffness (Fig. 3A). This initial rapid decrease in stiffness is believed to be directly related to PhoCl cleavage, which immediately weakens the gel network. The plateau stiffness that remains is hypothesized to be due to both incomplete cleavage of PhoCl, characterized in fig. S2 to reach a maximum of 75% cleavage, and entanglement of the protein chains. This rheological method only allows for the accurate capture of initial softening rather than the full gel-sol transition that would be indicated by a G'/G'' crossover as complete degradation relies on diffusion, which is highly restricted in parallel-plate rheology.

For comparison, we also tested the Coil protein developed in our previous work (elsewhere denoted as "PXP") (*9*), which has an identical structure to PhoCoil but lacks the PhoCl protein. As expected, Coil shows minimal change in stiffness when exposed to 405 nm over the same period of time, indicating that the photoresponsivity of PhoCoil stems directly from its mid-block PhoCl protein. The minimal softening of Coil captured over the course of photorheology is also seen without light exposure over the same interval and is expected to be a result of the gel swelling and eroding at the edges, as measurements are taken with the gel submerged in phosphate-buffered saline (PBS) (fig. S4).

To further probe PhoCoil's light-responsive properties, we exposed 10 wt % PhoCoil gels to intermittent and varying intensities of light. Here, we showed that PhoCoil softening is directly controlled by the time and intensity of light exposure and can be modulated as such. PhoCoil softening can be stopped before completion by removing light, resulting in immediate plateauing of the gel stiffness (Fig. 3B). The rate of gel softening can also be modulated by changing the intensity of the light, with higher intensities leading to more rapid softening to the same plateau value (Fig. 3C). Notably, the extent of softening scales directly with the total light dosage delivered (given in J cm^{-2}) regardless of the intensity of the source, with an intensity adjusted rate constant of 0.0451 ± 0.0005 cm^2 J^{-1} and half-life of 15.4 ± 0.2 $J \cdot cm^2$ for a 10 wt % gel (Fig. 3D). This relationship allows for simple calculation of the intensity of light and time of light exposure that can be used to reach a desired final stiffness if the initial gel stiffness is known.

Although we have demonstrated that partial softening can be achieved in a dose-dependent manner, there are some scenarios in which it may be useful to fix the minimum final stiffness that the material can be softened to. We hypothesized that this could be achieved by coformulating PhoCoil with our non–light-responsive Coil protein. These coformulated gels soften to intermediate final stiffnesses, with higher percentages of Coil leading to less softening despite receiving the same dosage of light (Fig. 3E).

To capture the complete degradation of PhoCoil gels, we turned to bulk degradation studies. PhoCoil gels at 7.5, 10, and 12.5 wt % were formed in microcentrifuge tubes and covered with excess PBS. The gels are initially green in color due to the inherent green fluorescence of PhoCl. Upon exposure to 405-nm light, the gels undergo a visible color change to orange as a result of the cleavage and rearrangement of PhoCl's chromophore, which occupies a red state before separation of the two halves of the protein (*10*) (Fig. 4A). We hypothesize that, because of the molecular crowding within the hydrogel, this separation is slowed, allowing the red state to persist longer than in solution. The gel then primarily erodes from the surface, where cleaved protein can more easily escape the network. Complete degradation is achieved in response to 405-nm light within 4 to 20 hours under these conditions, with increasing doses of light decreasing the time to complete degradation (Fig. 4, A and B). For gels kept in ambient light only (0-min light), no noticeable color change occurred through the duration of this experiment, indicating that PhoCl is resistant to photocleavage in ambient light. However, PhoCoil is susceptible to surface erosion in the absence of directed photocleavage as the network is only bound by dynamic, physical interactions. As such, coil exchange at the surface of the gel makes it possible for uncleaved polypeptides to diffuse away from the network while their coils are in an unbound state, as demonstrated with the Coil networks in a previous work (*9*). PhoCoil gels that are not exposed to 405-nm light persist for 3 days or longer under these conditions (Fig. 4A and fig. S5). Direct 405-nm light exposure substantially increased the rate of degradation; with 90 min of exposure to visible light (405 nm, 10 mW cm^{-2}), PhoCoil gels have half-lives that are 20 to 30 times shorter than those that are kept in ambient light (Fig. 4B and table S1). As expected, increasing the weight percentage of the network increases the average time to complete degradation for all light conditions.

Spatiotemporal control of gel softening and degradation

One substantial advantage of light as a stimulus is the ease of controlling its delivery spatiotemporally (*11*). Encouraged by our successful demonstration of PhoCoil's ability to photodegrade, we sought to control material dissolution in user-defined patterns (Fig. 5A). Here, we use photomask-based lithography to spatially control light exposure, resulting in clear patterns with micrometer-scale resolution (Fig. 5, B and C). The resulting patterns can easily be visualized with confocal microscopy by using the intrinsic color switch of PhoCl after cleavage. Intact, non–light-exposed areas have strong green fluorescence, whereas the photocleaved areas have increased red fluorescence. Photomask-based patterning can be achieved throughout a 500-μm-thick gel with good resolution at the ~100-μm scale (Fig. 5D). However, as pattern details get smaller, scattering of light within the hydrogel results in a reduction in pattern crispness and depth (Fig. 5, B and C).

We next used photomask-based lithography to spatiotemporally control complete gel degradation. To do so, we patterned gels with a variety of photomasks and then submerged them in a PBS bath with intermittent confocal imaging to capture various stages of degradation. Imaging showed that the light-exposed areas of the gels quickly degraded, whereas the unexposed areas persisted (Fig. 5E). Patterned degradation could be achieved in several configurations, including a

Downloaded from https://www.science.org on September 06, 2025

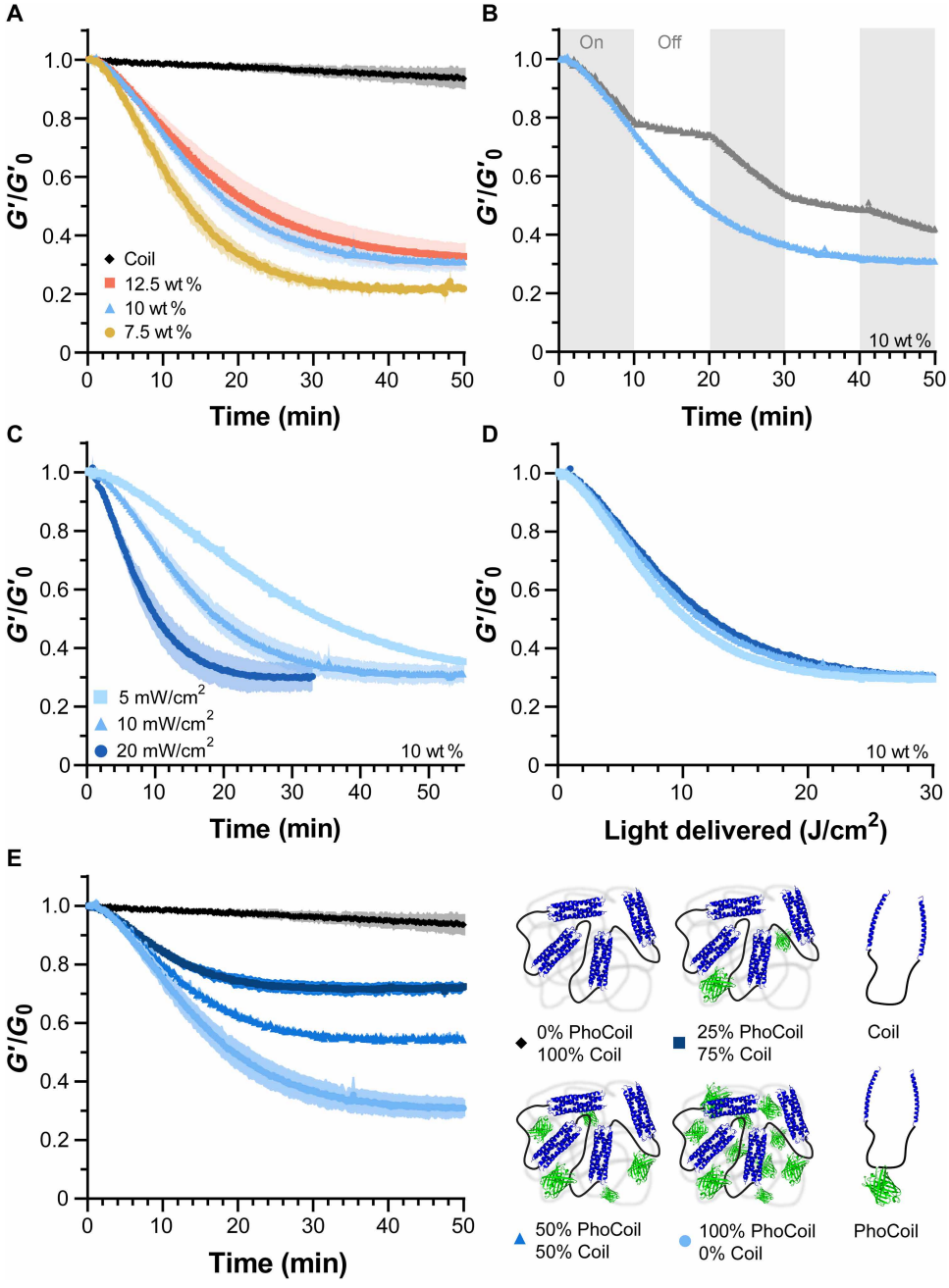

Fig. 3. Kinetics of PhoCoil gel photodegradation. (**A**) Gel softening in response to 405-nm light via oscillatory rheology time sweep. Rheology was conducted at 5% strain and 10 rad s^{-1} with light intensity set to 10 mW cm^{-2} at the gel. G'_0 was defined as the storage modulus immediately before light exposure. Three independent gels were measured for each weight percentage. Data are presented as the means (line) ± SD (shaded area). (**B**) Control of endpoint stiffness by modulation of light exposure time. Gels (10 wt %) were exposed to constant 10 mW cm^{-2}, 405-nm light (blue) or periods of 10-min light on, 10-min light off (gray). (**C**) Control of softening rate by modulation of light intensity. Three independent 10 wt % gels were measured for each intensity of 405-nm light. Data are presented as the means (line) ± SD (shaded area). (**D**) When normalized for light dosage, experimental data from (C) collapses onto a single curve, indicating that PhoCoil photocleavage follows the same light dose dependency for each intensity. (**E**) Control of endpoint stiffness by coformulation of PhoCoil with a non–light-responsive network-forming Coil protein. Three independent gels for each formulation were exposed to 10 mW cm^{-2}, 405-nm light, with the total molar concentration of protein kept constant across formulations. Data are presented as the means (line) ± SD (shaded area).

Downloaded from https://www.science.org on September 06, 2025

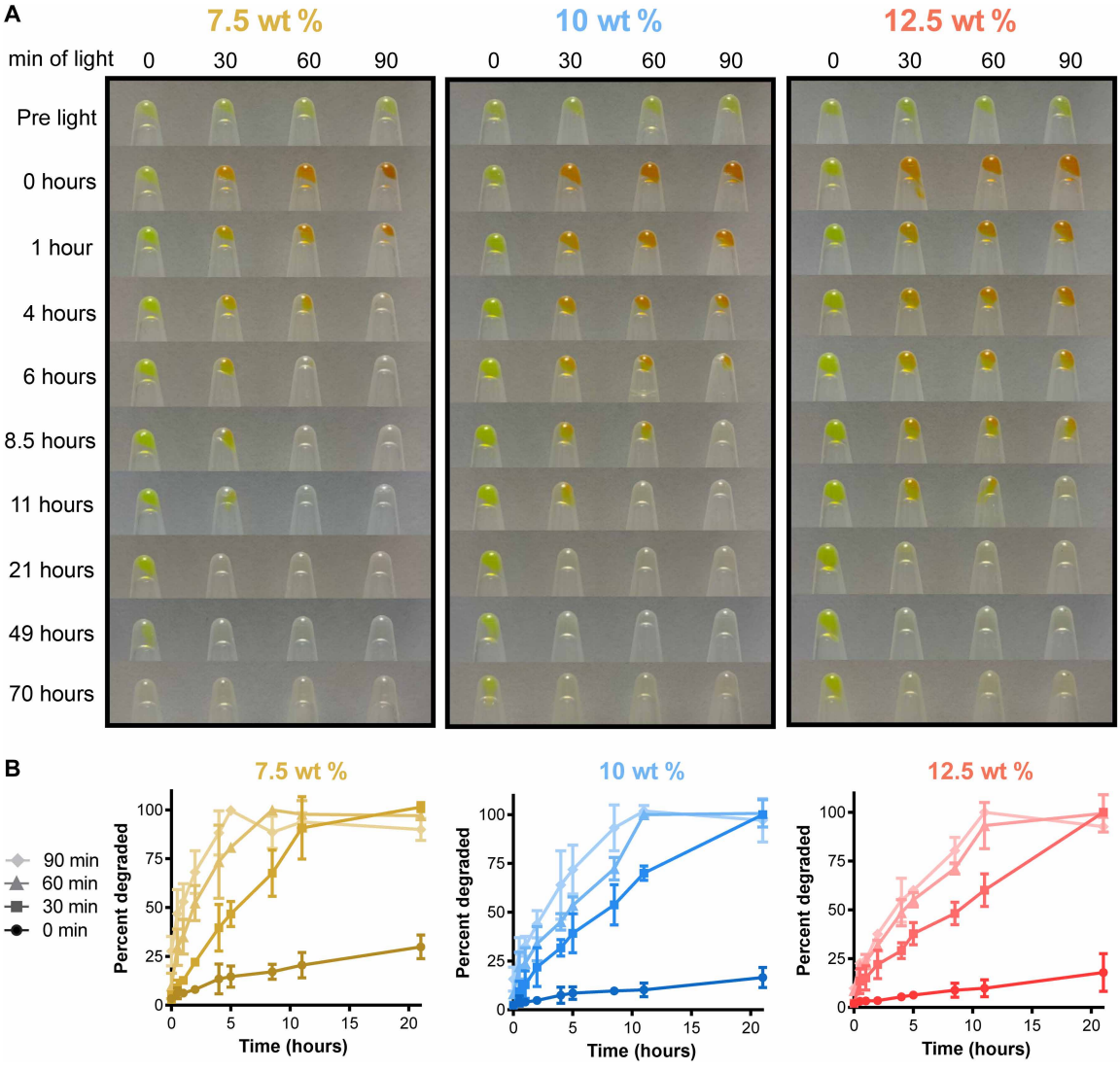

Fig. 4. Bulk degradation of PhoCoil gels. (**A**) Degradation of varying gel weight percentages in response to increasing time of light exposure. Gels (25 μl) covered with PBS were exposed to 10 mW cm^{-2}, 405-nm light for 0, 30, 60, or 90 min. Images of the remaining gel in inverted tubes were obtained at the indicated intervals postexposure. (**B**) Quantification of gel degradation rates. Samples of PBS above each gel were analyzed by BCA assay to determine the protein content as a measure of the percentage of gel degraded at each interval postexposure. Three independent gels were tested for each combination of weight percentage and light exposure time. Data shown are means ± SD.

half gel, central "W," and central circle. Sequential light exposures permitted staged degradation of different sections of the material.

To determine whether controlled photodegradation could be achieved in tissue, we used ex vivo tissue (deli turkey or skin-on chicken) as a barrier for light to pass through to reach the PhoCoil gel (Fig. 5F). Degradation of the unmasked sections of these gels was easily achieved under thin tissue sections (~1 to 2 mm), demonstrating that PhoCoil gels may be useful for controlled therapeutic delivery at low injection depths (Fig. 5G and fig. S6).

Photodegradation of gels in vivo

Following our successful demonstration of PhoCoil photodegradation through ex vivo tissues mimic, we sought to replicate these findings in an in vivo mouse model. Each animal received two dorsal subcutaneous gel injections, and the fluorescence in both green and red wavelengths was measured using an in vivo imaging system (IVIS) to track intact and photocleaved gel, respectively. The injection site on the right side of each animal was subsequently exposed to 405-nm light to induce gel degradation, and IVIS was repeated (Fig. 6A). The injection site on the left side was not exposed to light. Similar light exposure conditions, sometime repeated over several sessions, have previously demonstrated utility in both mice and humans for treatment of a variety of skin diseases with few side effects (*51*–*53*).

IVIS images showed that, before light exposure, both injection sites had similar levels of green fluorescence and no red fluorescence, indicating that gels remained fully intact (Fig. 6, B and C, and fig. S7, A to D). After light exposure, a statistically significant decrease in green signal and increase in red signal can be seen at the site that received light, whereas the untreated site shows no change

Downloaded from https://www.science.org on September 06, 2025

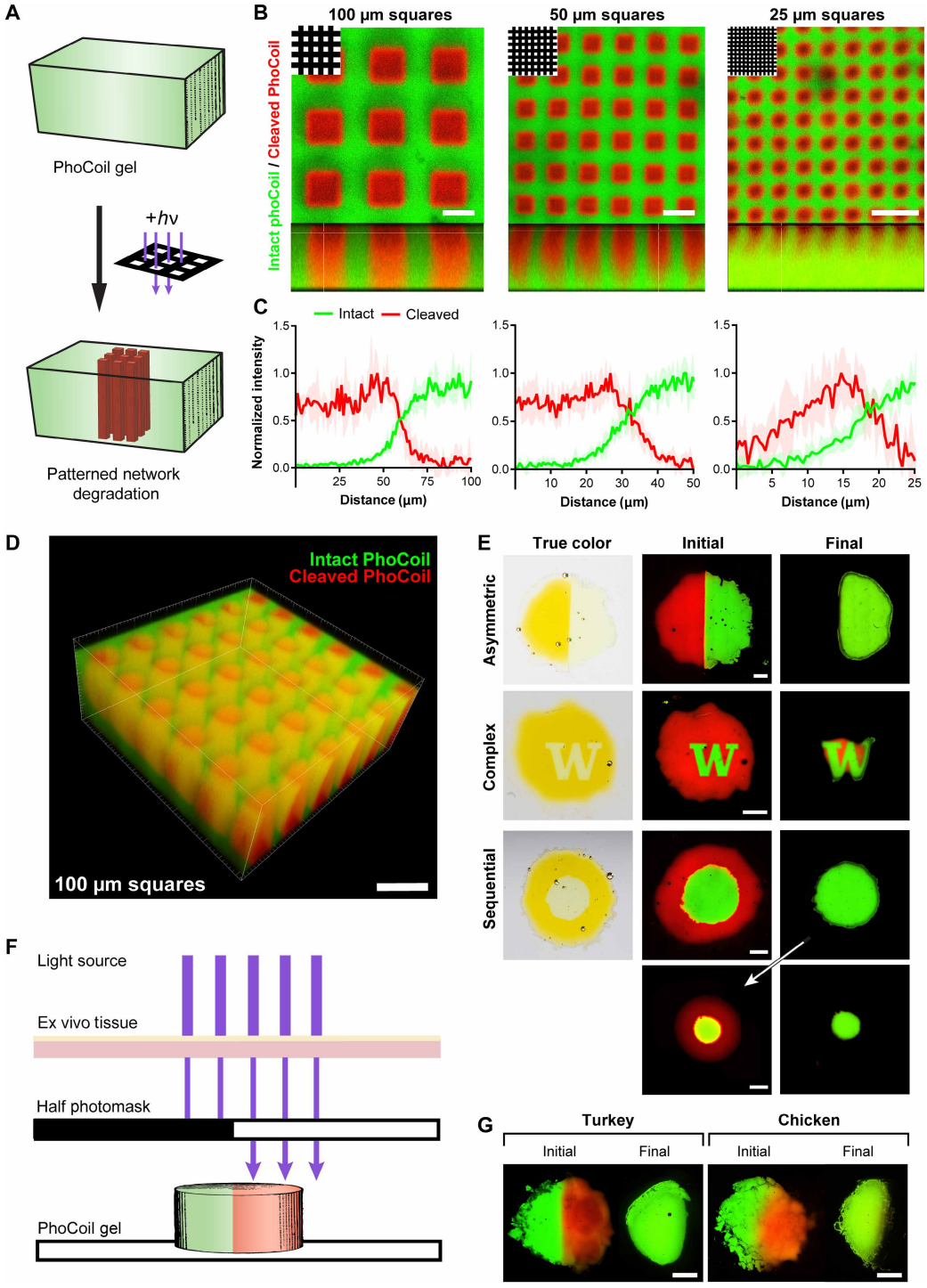

Fig. 5. Photopatterning and spatially controlled degradation of PhoCoil gels. (**A**) PhoCoil gels can be patterned using photomasks to restrict 405-nm light to desired areas. (**B**) Photomask-based patterning of grids of varying sizes onto PhoCoil gels. Gels were exposed to 60 min of 10 mW cm^{-2}, 405-nm light through a grid photomask with light passing through 100-, 50-, or 25-µm-wide squares (top left). Images were obtained in the *xy* (top) and *xz* (bottom) planes via confocal microscopy. Scale bars, 100 µm. (**C**) Intensity in red and green channels was quantified via ImageJ to demonstrate changes in resolution of patterning. Intensity was quantified from the center of a red square to the center of a green line at five random locations. Data shown are means ± SD. (**D**) 3D reconstruction of the 100-µm grid pattern throughout the thickness of a gel. Scale bar, 250 µm. (**E**) Spatially controlled degradation of photomask patterned gels. Gels were exposed to 60 min of 10 mW cm^{-2}, 405-nm light through a photomask and then photographed (true color) or confocal imaged (initial). Gel degradation was allowed to occur in excess PBS, and gels were confocal imaged to visualize degradation (final). Scale bars, 1 mm. (**F** and **G**) Light-based degradation of PhoCoil gels through ex vivo tissue. The left half of each gel was covered with a photomask, and the entire gel was placed under 1-mm-thick deli turkey or chicken skin. Gels were exposed to 5 min of high-intensity 405-nm light through the tissue mimic, confocal imaged to visualize the pattern (initial), and left to degrade in excess PBS before final fluorescent imaging. Scale bars, 1 mm.

Downloaded from https://www.science.org on September 06, 2025

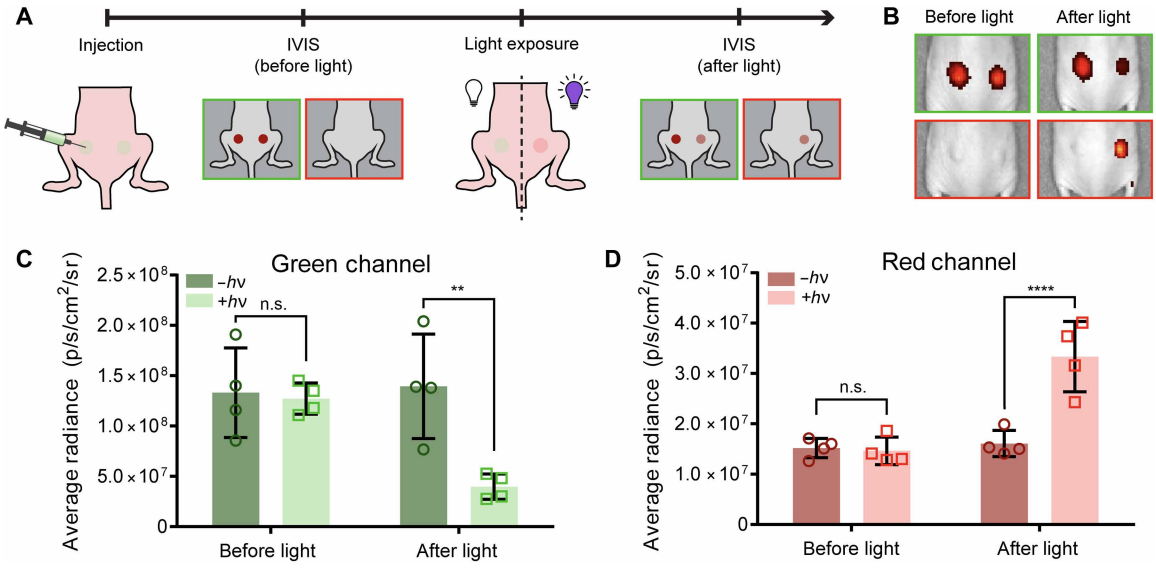

Fig. 6. In vivo degradation of PhoCoil gels. (**A**) Animals were injected with PhoCoil gel subcutaneously on both the left and ride sides of the dorsal region. IVIS images were taken to detect green (intact gel) and red (cleaved gel) fluorescence before light exposure. Subsequently, the right side of each animal was exposed to 405-nm light to initiate gel degradation. IVIS imaging was repeated after light exposure. (**B**) Representative IVIS images taken before and after light exposure. Images outlined in green represent green fluorescence, and those in red represent red fluorescence of the injected gels. (**C**) Quantification of green fluorescence before and after light. (**D**) Quantification of red fluorescence before and after light. Darker bars represent gels on the left side of each animal, which did not received light. Lighter bars represent gels on the right side of each animal, which did receive light. All bars represent the means ± SD for four animals. Significance testing was performed using Sidak's multiple comparisons test. n.s., not significant; *$P < 0.05$, **$P < 0.01$, ***$P < 0.001$, ****$P < 0.0001$.

in either signal (Fig. 6, B and C). The drop in green signal and appearance of the red signal is expected following photocleavage of PhoCoil. By day 7 postinjection, there remain detectable levels of green fluorescence by IVIS, indicating that intact PhoCoil is still present. However, all red fluorescence has dissipated, indicating that all cleaved PhoCoil has degraded and that light exposure decreases degradation time. This was confirmed on explant of the gels (fig. S7E). Furthermore, analysis of 405-nm light intensity through excised mouse skin indicates that ~14.6% of light penetrates to this depth, which may be useful in determining light exposure conditions for future studies (fig. S7F). Overall, these results indicate that photodegradation of PhoCoil can be achieved transdermally, further supporting its utility in controlled delivery.

Biocompatibility of gels in vivo

Utilization of PhoCoil gels in vivo also requires that these materials be highly biocompatible. To assess biocompatibility of PhoCoil, we evaluated the local and systemic inflammatory responses to gel injection in immune-intact syngeneic C57BL/6 mice. To allow for localization of the gels throughout the study and analysis, mice were implanted with MC38 tumors in their flanks and gels were injected directly into the tumors. Forty-eight hours after gel injection, tissues and blood were harvested for analysis (Fig. 7A). Inflammatory responses to PBS, HyStem gel, and Coil gel were all assessed for comparison of PhoCoil to a vehicle control, a Food and Drug Administration–approved hydrogel for cell delivery, and a nonphotoresponsive coiled-coil protein hydrogel, respectively. To assess the systemic inflammatory response, mouse body weight was measured over 48 hours after gel injection. We observed no significant animal weight changes, indicating that PhoCoil did not induce a strong inflammatory response (Fig. 7B). To further quantitatively assess the systemic response, cytokine analysis of the harvested blood was carried out. No significant difference in cytokine levels was observed between across all injection types, indicating that PhoCoil does not elicit a substantial systemic inflammatory response (Fig. 7C).

To evaluate the local inflammatory response, we performed hematoxylin and eosin (H&E) staining and immunohistochemistry (IHC) on the harvested MC38 tumors. No signs of inflammation or fibrosis were observed in any injection condition by H&E. To further confirm the lack of acute local inflammation, IHC was used to examine the presence of macrophages, neutrophils, dendritic cells, natural killer (NK) cells, and T cells. Compared to all three control groups, none of the immune cell populations we investigated appeared to be up-regulated in the PhoCoil group (Fig. 7D). This suggests that PhoCoil does not induce a local inflammatory response within 48 hours of injection. Collectively, the lack of a local or systemic inflammatory response demonstrates that PhoCoil is highly biocompatible.

Cell viability through encapsulation, injection, and light-mediated release

Given our success in demonstrating injectability, photodegradation, and biocompatibility of PhoCoil, we lastly aimed to assess its potential utility in cell delivery. In our previous work with the Coil system, we demonstrated that Coil gels support high cell viability through encapsulation and injection, both in vitro and in vivo (*9*). As the PhoCoil gels are formed in an identical manner to Coil gels, it remains straightforward to encapsulate cells in PhoCoil gels. Cells in the suspension (viability of >99%) are combined with the PhoCoil protein to yield encapsulated cells, which retained 85% viability at 1.5 hours postencapsulation (Fig. 8, A to D). For cells encapsulated in PhoCoil and subsequently injected through a 25-gauge needle, 79% viability was observed (Fig. 8, B and E).

Downloaded from https://www.science.org on September 06, 2025

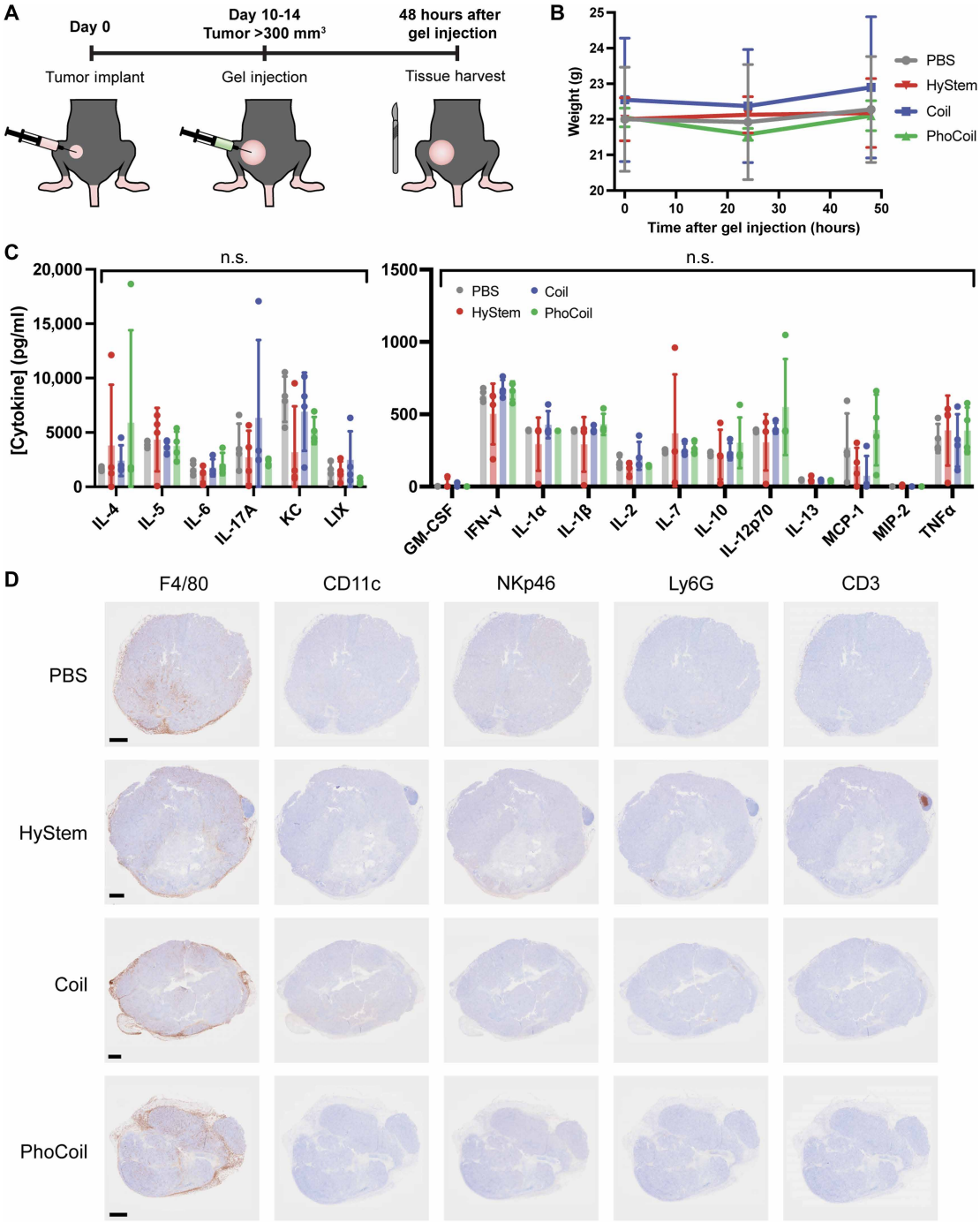

Fig. 7. Biocompatibility of PhoCoil gels in vivo. (**A**) MC38 flank tumors were established, followed by intratumoral injection of PBS, HyStem gel, Coil gel, or PhoCoil gel. Forty-eight hours after injection, the tumor and whole blood were harvested for inflammatory response analysis. (**B**) Animal weight was monitored immediately after PBS/gel injection and at 24 and 48 hours after injection. All bars represent the means ± SD of $n = 4$ animals. (**C**) An inflammatory cytokine array was performed on whole blood collected from each animal to detect potential systemic inflammatory responses. All bars represent the means ± SD of $n = 4$ animals. Significance testing was done using a one-way ANOVA. n.s., not significant. (**D**) IHC was performed on tumor tissue to detect potential local inflammatory responses. Scale bars, 1 mm.

Unlike our previously developed Coil system, cells encapsulated in PhoCoil hydrogels can be subsequently released using visible light to liberate single-cell suspensions at a user-defined time point. To demonstrate this, encapsulated cells were exposed to 405-nm light to induce gel photodegradation. Photoreleased cells were then left for 2 days to encourage readherence to the dish and proliferation before imaging. These cells retained their proliferative capacity and expanded to cover a tissue culture plate over this 2-day period (Fig. 8F). Given PhoCoil's ability to support high cell viability throughout injection and photodegradaton, it is poised for applications in therapeutic cell delivery, where it can provide a protective matrix for cells that will degrade slowly overtime or quickly after light exposure.

Downloaded from https://www.science.org on September 06, 2025

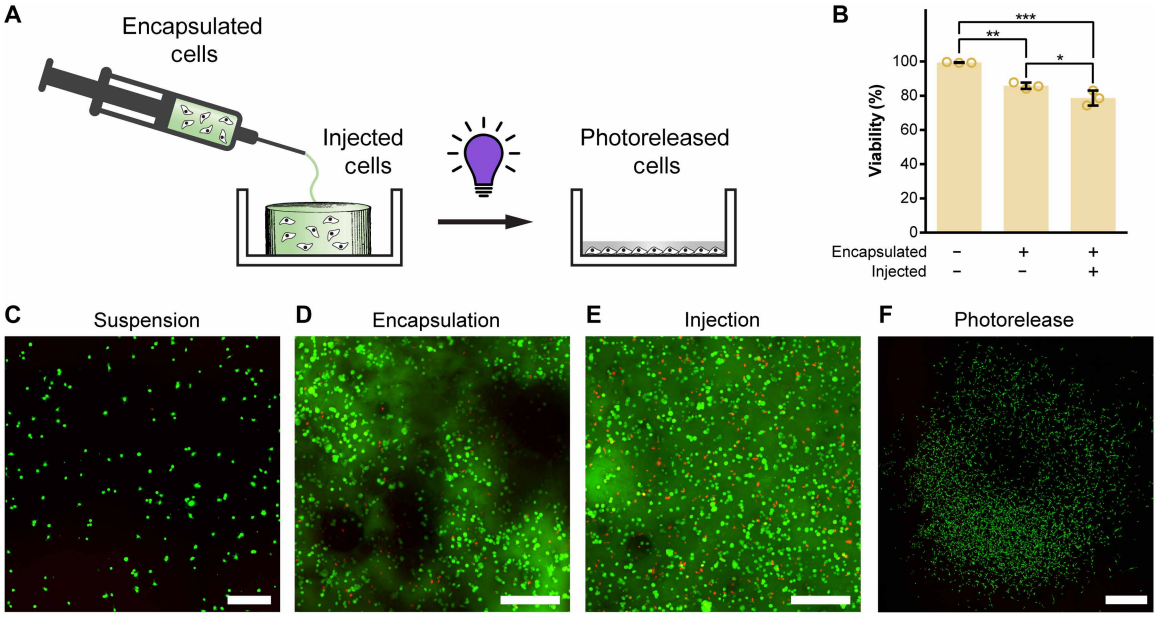

Fig. 8. Viability of PhoCoil-encapsulated fibroblasts. (**A**) 10T1/2 fibroblasts are encapsulated in the gel, injected into a well plate, and released from the gel via 405-nm light. (**B**) Viability of 10T1/2 fibroblasts throughout mock processing (in the suspension, after encapsulation in the gel, and after injection in the gel) for therapeutic cell delivery in PhoCoil gels. All bars represent the means ± SD of three independent gels for each condition. Significance testing was done using Tukey's multiple comparisons test. (**C**) Representative confocal microscopy image of Live/Dead analysis of 10T1/2 fibroblasts in the suspension. Scale bar, 250 μm. (**D**) Representative confocal microscopy image of Live/Dead analysis of 10T1/2 fibroblasts postencapsulation in a 7.5 wt % PhoCoil gel. Image is a maximum projection of a *z*-stack through a 0.5-mm-thick gel. Scale bar, 250 μm. (**E**) Representative confocal microscopy image of Live/Dead analysis of 10T1/2 fibroblasts postinjection in a 7.5 wt % PhoCoil gel. Image is a maximum projection of a *z*-stack through a 0.5-mm-thick gel. Scale bar, 250 μm. (**F**) Representative confocal microscopy image of Live/Dead-stained 10T1/2 fibroblasts released from a PhoCoil gel. Cells were subjected to encapsulation and injection, followed by release from the gel into a cell culture dish using 405-nm light exposure. Two days following release, cells were stained and imaged to assess their ability to survive and proliferate after such handling. Scale bar, 1 mm. $*P < 0.05$, $**P < 0.01$, $***P < 0.001$.

DISCUSSION

In this work, we have showcased the unique properties of PhoCoil, a single-component recombinant protein hydrogel system that is biocompatible, injectable, and photodegradable. The molecular design of the PhoCoil protein allowed us to preemptively engineer in our desired properties to realize this dynamic material. PhoCoil forms supramolecular hydrogels that with tunable stiffnesses spanning that of many native tissues, and its injectability primes it for applications in minimally invasive, controlled therapeutic delivery. Furthermore, the photoresponsivity of PhoCoil allows for its softening and degradation to be bioorthogonally and spatiotemporally controlled in a precise and dose-dependent manner. We showed that this photodegradation can be achieved under thin layers of ex vivo tissue as well as subcutaneously in vivo, suggesting its potential utility for transdermally triggered dissolution. Notably, PhoCoil is susceptible to slow degradation over time in the absence of light, owing to its physically cross-linked nature and bioresorbability, but direct photodegradation of PhoCoil results in much more rapid material dissolution. Last, we demonstrated that PhoCoil gels are biocompatible; they do not elicit an inflammatory response and support high viability of encapsulated cells, opening up their application to cell-based therapeutics and regenerative medicine applications. Collectively, this work provides proof-of-concept evidence of PhoCoil's potential utility in therapeutic cell delivery.

To take advantage of PhoCoil's photodegradability for rapid material dissolution in a biomedical context, it is best positioned for intradermal or subcutaneous therapeutic delivery or for applications in more optically transparent tissues (e.g., eyes). However, substantial advances in protein engineering and de novo protein design may enable the development of further red-shifted variants of PhoCl (*54*, *55*). This would be particularly useful as longer wavelengths of light penetrate deeper through tissue (*56*, *57*). Furthermore, continued development of tools that allow shorter wavelengths of light to penetrate deeper into the body, such as upconverting nanoparticles, implantable light-emitting diodes, and optical waveguides (*57*–*60*), offer exciting opportunities for combinatorial approaches that would further enable in vivo regulation of PhoCoil and other light-responsive materials.

As cell-based therapies continue to be a focus of next-generation therapeutic approaches, hydrogels will surely play a role in their development and effective implementation (*61*). Recombinant protein–based materials, such as PhoCoil, are well positioned to be used for translational therapies given their perfectly defined, tunable, and bioresorbable nature. Recent advances in de novo protein design have also enabled development of self-associating proteins not seen in nature, opening up additional possibilities for design of genetically encoded protein biopolymer networks (*62*). The recent emphasis in biotech on protein-based therapeutics promises to develop more efficient and cost-effective ways to screen protein expression conditions and achieve large-scale protein expression, which will further enable the usage of such recombinant protein materials (*63*, *64*).

Downloaded from https://www.science.org on September 06, 2025

MATERIALS AND METHODS

Cloning

A gBlock (IDT) containing the sequence encoding 6xHis-RGD-Coil-XTEN-PhoCl2c-XTEN-Coil-RGD-6xHis, herein referred to as PhoCoil, was inserted into the pET21 vector via Gibson assembly (NEB). This plasmid is available through Addgene (ID 220444). The resulting mixture was transformed into TOP10 *Escherichia coli*, and the sequence was confirmed by Sanger sequencing (Genewiz). The plasmid was then transformed into electrocompetent BL21(DE3) *E. coli* for protein expression work.

Protein expression

BL21(DE3) *E. coli* containing the pET21 PhoCoil plasmid was grown overnight in lysogeny broth (LB). Fresh LB medium was combined with carbenicillin and inoculated 1:200 with the overnight culture. The culture was grown at 37°C and 210 rpm, and the OD_{600} (optical density at 600 nm) was monitored until 0.4 to 0.6, at which point 0.5 mM isopropyl-β-D-thiogalactopyranoside (IPTG) was added and the culture was moved to 18°C and 210 rpm for 24 hours in the dark. Cells were harvested by centrifugation of 500 ml of culture at 4000*g* for 20 min at 4°C. Cell pellets were frozen at −80°C at least overnight. Coil protein (*9*) was expressed following the same protocol.

Protein purification

Cell pellets, each derived from 500 ml of culture, were resuspended in 40 ml of lysis buffer [50 mM NaCl, 20 mM Tris, and 10 mM imidazole (pH 8)] supplemented with 1 mM phenylmethylsulfonyl fluoride (PMSF). Resuspended cells were placed in an ice water bath and sonicated at 30% amplitude for 6 min of total on time in 1-s on and 2-s off intervals (Fisherbrand, model 505 Sonic Dismembranator, 0.5-inch probe). The cell lysate was centrifuged at 10,000*g* for 20 min at 4°C, and the supernatant was collected and stored at 4°C for 7 days to encourage full chromophore maturation of PhoCl. The clarified lysate was again centrifuged at 10,000*g* for 20 min at 4°C, and the supernatant was collected for purification. Ni-NTA HisTag affinity chromatography was conducted using an ÄKTA Pure 25L with a 5-ml HisTrap column (Cytiva). Forty milliliters of the clarified cell lysate was loaded onto the column. The column was then thoroughly washed [50 mM NaCl, 20 mM Tris, and 15 mM imidazole (pH 8)], and the protein was eluted [100 mM NaCl, 40 mM Tris, 500 and mM imidazole (pH 7.5)]. Collected elution fractions containing the protein were desalted into water using a 50-ml 26/10 desalting column (Cytiva) on the ÄKTA. The column was equilibrated with deionized water, and 13 ml of the collected elution was loaded, followed by elution with deionized water. Only the protein peak (high A280 and low conductivity) was collected, flash-frozen in liquid nitrogen, and lyophilized for 3 days. The lyophilized protein was stored in parafilm-wrapped tubes at −20°C.

Gel formation

Gels were formed by resuspending the lyophilized protein in sterile 10X PBS (pH 7.4) at 7.5, 10, or 12.5 wt %. Each milligram of protein was assumed to take up 1 μl of volume in the mixture. Immediately after PBS addition, tubes were placed at 37°C for 5 min. The mixture was then thoroughly stirred with a pipette tip to break up chunks of protein and returned to 37°C for 20 min, at which point a cohesive gel was observed. The gels were centrifuged at 10,000*g* for 5 min to remove trapped bubbles and placed at 4°C on a rocker overnight before use.

To form PhoCoil/Coil mixed gels, the ratio of each component was determined on a molar basis. All gels contained a total of 1.71 mM protein, benchmarked to a 10 wt % 100% PhoCoil gel. Each protein component was weighed out and combined in a single tube, and gels were prepared as described above.

Rheology

Rheology was performed on an Anton Paar Physica MCR 301 using an 8-mm-diameter parallel-plate geometry with a 0.5-mm gap, at 25°C. Approximately 60 μl of the preformed gel was loaded and covered with mineral oil to prevent evaporation. The following testing routine was performed on each gel: time sweep (10 rad s^{-1}, 5% strain, 30 min), frequency sweep (0.1 to 50 rad s^{-1}, 5% strain), time sweep (10 rad s^{-1}, 5% strain, 10 min), strain sweep (10 rad s^{-1}, 0.1 to 500% strain), time sweep (10 rad s^{-1}, 5% strain, 10 min), cyclic strain sweep (10 rad s^{-1}, 5% strain for 5 min and then 500% strain for 30 s, repeated four times total), time sweep (10 rad s^{-1}, 5% strain, 10 min), and shear sweep (0.1 to 50 s^{-1} shear rate). G' values were determined by averaging all measurements in the initial time sweep. Crossover strain values were determined through linear interpolation.

Photorheology

Photorheology was performed on an Anton Paar Physica MCR 301 using an 8-mm-diameter parallel-plate geometry and a custom, optically transparent lower plate with a fitting for a light guide. All measurements were performed with a 0.5-mm gap at ambient temperature, with the frequency held at 10 rad s^{-1} and strain at 5%. Preformed gels were covered with excess PBS (pH 7.4) and allowed to swell for 1 to 2 hours. Gels were then loaded onto the rheometer and trimmed with plastic tweezers to the edge of the geometry. The well in the custom plate was filled with 5 ml of PBS to prevent the gel from drying out or heating up during the run. The gel was allowed to equilibrate and stiffness plateau for 15 min, at which point the light source (Mightex WheeLED, 405 nm, 5 to 20 mW cm^{-2} at the gel) was turned on for 50 min to capture gel softening. For the interval light exposure, the light was turned on for 10 min and then off for 10 min for a total of 50 min. The final G' value before light exposure was set as G'_0.

Bulk degradation study

Gel degradation behavior was assessed in PBS with and without light exposure. Preformed 25-μl gels in 1.5-ml microfuge tubes were washed twice with 1 ml of PBS and then covered with 1 ml of PBS (pH 7.4). Gels were then exposed to 405-nm light at 10 mW cm^{-2} for 0, 30, 60, or 90 min, with tubes rotated 180° every 15 min to ensure uniform light exposure. Tubes were then placed in a shaker incubator at 37°C and 150 rpm, with the tubes oriented parallel to the shaker plate. Images of the gels and aliquots of the PBS above the gels were taken over the course of 3 days. Each time, fresh PBS was added to each tube to maintain a constant volume. The protein concentration of each sample was determined by BCA assay (Thermo Fisher Scientific, Pierce BCA Protein Assay Kit) relative to a bovine serum albumin (BSA) standard curve. Data were adjusted to account for evaporation over the course of the study on the basis of the volume of liquid remaining at the end of the study and assuming linear volume loss. Values were normalized to from 0 to 100%, with the 100% point selected on the basis of cross-referencing the data with the provided images of the gels. Half-lives were determined from the first-order rate constant, calculated for each replicate, and averaged.

Downloaded from https://www.science.org on September 06, 2025

Photomask-based patterning and degradation

Preformed gels were divided into 5- to 10-μl volumes using plastic tweezers and placed onto a glass slide. Rubber spacers (0.5 mm thick) were placed on each side of the gel, and a coverslip was placed on top to flatten the gel into a disc. The remaining empty space between the slide and coverslip surrounding the gel was filled with PBS (pH 7.4) to keep the gel hydrated. The mounted gel was oriented with the coverslip touching the photomask, and the glass slide was covered with a piece of black rubber to prevent residual light passing through the gel from backscattering. A 405-nm light source was oriented to shine through the photomask and onto the gel with a power of 10 mW cm^{-2} at the gel surface. Light exposure was maintained for 1 hour, at which point the gels were imaged on a Leica Stellaris 5 confocal microscope to visualize the resultant pattern. Intact PhoCoil (green) was visualized with an excitation wavelength of 489 nm and an emission detection range of 494 to 572 nm. Cleaved PhoCoil (red) was visualized with an excitation wavelength of 587 nm and an emission detection range of 592 to 750 nm. To quantify the patterning resolution of the grids, images were analyzed in ImageJ. A line was drawn from the center of light exposed region to the center of a non–light-exposed region, and the value of the green and red channels over this line were determined using the plot profile tool. This was repeated five times per grid size at random locations in the image. For 3D images, *z*-stacks were reconstructed in ImarisViewer. For photodegradation, patterned gels were imaged immediately after light exposure, and then the entire slide was placed in a bath of PBS in an incubator shaker at 37°C and 100 rpm. Gels were intermittently imaged to capture degradation of the light exposed areas of the gel.

Ex vivo photodegradation

Preformed gels were prepared between glass slides as detailed above. Half of the gel was covered with a rubber photomask, and the whole gel was covered with the indicated tissue (deli turkey or skin-on chicken). A 405-nm light source was set up ~1 mm above the tissue. The following conditions were used: 1 mm of deli turkey, 150 mW at source, 5-min exposure; 2 mm of deli turkey, 150 mW at source, 10-min exposure; 2 mm of deli turkey, 25 mW at source, 60-min exposure; chicken skin alone (1 mm), 125 mW at source, 5-min exposure; and 2 mm of chicken with skin on 125 mW, 15-min exposure. The tissue was intermittently sprayed with deionized water to keep it from drying. Immediately after light exposure, gels were imaged by confocal microscopy as noted above. Each slide was then placed in a bath of PBS overnight at ambient temperature, and confocal image of the remaining gel was captured.

In vivo injection and photodegradation

Previously purified PhoCoil protein stored in solution at −80°C was thawed and repurified via Ni-NTA HisTag affinity chromatography to remove endotoxin. Identical purification conditions were used as noted in the protein purification section above but with the addition of an endotoxin wash step [50 mM NaCl, 20 mM Tris, 15 mM imidazole, and 0.1% Triton X-114 (pH 8)] after lysate loading and before typical washing. Collected elution fractions were desalted as noted above, and the collected protein was 0.2-μm filtered for sterility, flash-frozen in liquid nitrogen, and lyophilized. PhoCoil gels (5 wt %) were formed under sterile conditions in a tissue culture hood by resuspending the lyophilized protein in sterile 10X PBS (pH 7.4), followed by incubation at 37°C for with intermittent mixing via the pipette tip for ~1 hour. Once gel formation was completed, the material was transferred by micropipette to a 0.5-ml syringe fitted with a 26-gauge needle. All surgical procedures were approved by the Institutional Animal Care and Use Committee at the University of Washington (PROTO201600331). Taconic NCr nude mice (female, 9 to 10 weeks old, four mice in total) were anesthetized using isoflurane. Twenty-microliter gel injections into the subcutaneous space of the left and right dorsal regions (two injections per animal) were delivered. Animal recovery from surgery was monitored, and animals were administered meloxicam (5 mg kg^{-1}) subcutaneously postoperation for 3 days. Mice were imaged using an In Vivo Imaging System (IVIS) Spectrum imaging system (PerkinElmer) per the manufacturer's protocol to capture fluorescence at an excitation/emission of 465/520 nm for the green channel and 570/620 nm for the red channel after injection. Following imaging, the right side gel was exposed to 65 J cm^{-2} of 405-nm light and imaging was repeated to capture differences after light exposure. Imaging was repeated for several days following the injection to track gel degradation.

In vivo local inflammatory response testing

The MC38 flank tumor mouse model was prepared by subcutaneous injection of 2.5×10^5 MC38 murine colon adenocarcinoma cells (Sigma-Aldrich, #SCC172) in 100 μl of PBS into the flank of C57BL/6-Elite (SOPF) mice (Charles River Laboratories, #475, female, 9 to 10 weeks old, four mice per group). When the tumor volume reached 300 mm^3, as measured by vernier calipers, 20 μl of PBS, PhoCoil, Coil (*9*), or HyStem (Advanced BioMatrix, #GS310F) gels was injected intratumorally using 27-gauge insulin syringes. PhoCoil and Coil gels (5 wt %) were prepared under sterile conditions in a tissue culture hood by resuspending the lyophilized protein in sterile 1X PBS (pH 7.4), followed by incubation at 37°C with intermittent mixing via the pipette tip for ~1 hour. Once gel formation was completed, the material was transferred by a spatula to a 0.5-ml 27-gauge insulin syringe. The HyStem hydrogel was prepared by following the manufacturer's protocol. Briefly, as soon as HyStem and Extralink were mixed with 1X PBS, the mixture was loaded into a 0.5-ml 27-gauge insulin syringe and incubated at 37°C. Forty-eight hours after injection, the tumor was harvested and fixed with formalin and 70% ethanol. All murine procedures were approved by the Seattle Children's Research Institutional Animal Care and Use Committee (PROTO201600331). Inflammatory response of the gels was evaluated by IHC against F4/80, CD11c, CD3E, Ly6G, and NKp46. Paraffin sections were cut at 4 μm, air-dried at room temperature overnight, and baked at 60°C for 1 hour. Slides were stained on a Leica BOND Rx autostainer (Leica, Buffalo Grove, IL) using Leica Bond reagents. Endogenous peroxidase was blocked with 3% H_2O_2 for 5 min followed by protein blocking with TCT buffer (50 mM Tris, 150 mM NaCl, 0.25% casein, 0.1% Tween 20, and 0.05% ProClin 300 at pH 7.6) for 10 min. Primary antibodies were incubated for 1 hour, and polymers were applied as shown in Table 1, followed by Mixed Refine DAB (Leica DS9800) for 10 min and counterstaining with Refine Hematoxylin (Leica DS9800) for 4 min. After staining, slides were dehydrated, cleared, and coverslipped with permanent mounting media.

In vivo systemic inflammatory response testing

Systemic inflammatory responses were assessed by measuring blood cytokine concentrations. C57BL/6-Elite (SOPF) mice bearing subcutaneous flank MC38 tumors were injected with 20 μl of PBS or gel as described in the previous section. At 48 hours, whole blood was

Downloaded from https://www.science.org on September 06, 2025

Table 1. Information for IHC studies. HRP, horseradish peroxidase.

Antibody	Host	Clone	Manufacturer	Catalog no.	Dilution	Secondary polymer
F4/80	Rabbit	D2S9R	Cell Signaling Technology	70076	1:2000	12-min PowerVision Rabbit HRP polymer
CD11c	Rabbit	EPR21826	Abcam	Ab219799	1:100	12-min PowerVision Rabbit HRP polymer
Ly6G	Rat	1A8	BioLegend	127602	1:2000	60-min PowerVision Rat HRP polymer
NKp46	Rabbit	EPR23097-35	Abcam	Ab233558	1:200*	12-min PowerVision Rabbit HRP polymer
CD3	Rabbit	EPR20752	Abcam	Ab215212	1:7000	12-min PowerVision Rabbit HRP polymer

*This protocol uses high salt washes after application of the primary antibody to enhance staining.

collected via cardiac puncture into EDTA-coated tubes. Blood samples were stored at −80°C. A panel of inflammatory cytokines, including granulocyte-macrophage colony-stimulating factor (GM-CSF), interferon-γ (IFN-γ), interleukin-1α (IL-1α), IL-1β, IL-2, IL-4, IL-5, IL-6, IL-7, IL-10, IL-12p70, IL-13, IL-17A, keratinocyte-derived cytokine (KC/CXCL1), lipopolysaccharide-induced CXC chemokine (LIX), monocyte chemoattractant protein-1 (MCP-1), macrophage inflammatory protein-2 (MIP-2), and tumor necrosis factor–α (TNFα), were quantified using the Mouse High Sensitivity T-Cell 18-Plex Discovery Assay Array (Eve Technologies, MDHSTC18).

Cell viability

Cell viability during encapsulation and injection was assessed using 10T1/2 fibroblasts. Cells (passage 8) were cultured in dishes until ~70% confluent and then treated with TrypLE to obtain a single-cell suspension. Cells were pelleted and then suspended in FluoroBrite medium supplemented with 10% FBS, 1x penicillin-streptomycin, and 25 mM Hepes at >2 million cells ml^{-1}. For the suspension condition (−encapsulation and −injection), the cell suspension was dispensed into a tissue culture dish and stained with 2 μM calcein AM and 1 μM ethidium homodimer for 30 min before imaging. For the gel conditions (+encapsulation and ±injection), the cell suspension and fresh media were used to resuspend lyophilized PhoCoil to obtain 7.5 wt % gels with 2 million cells ml^{-1} of gel. After combining, the mixture was placed at 37°C for 10 min and then mixed by stirring with a pipette tip to ensure a homogeneous suspension of cells in the gel. This was repeated three more times, and then the mixture was briefly centrifuged to gather the gel at the bottom of the tube. Gels were dispensed by positive displacement pipette (−injection) or through a Hamilton syringe with a 0.4″-long, 20-gauge needle (+injection) into rubber molds placed in 30-mm dishes. These molds had circular cavities 0.5 mm deep and 10 μl in volume to hold the gels. Three gels (10 μl) were placed in each dish and covered with 8 μM calcein AM and 2 μM ethidium homodimer in PBS for Live/Dead analysis. Gels were incubated at 37°C in stain for 1.5 hours before imaging on a Leica Stellaris Confocal Microscope to visualize cells. *Z*-stacks thorough the thickness of the center of each gel were obtained, and maximum intensity *z*-projections of each were used to quantify cell viability by manually counting live (green) and dead (red) cells. For light-mediated cell release, molds were removed from around the gels, which were then covered with 100 μl of fresh media. A 405-nm light (100 mW at source) was positioned directly above the dish lid over the gel for 10 min. Photodegraded gels were then covered with additional Dulbecco's modified Eagle's medium (DMEM) and incubated for 2 days to allow for cell growth. After 2 days, the media were supplemented with 2 μM calcein AM and 1 μM ethidium homodimer and cells were allowed to stain for 30 min before imaging.

Statistical analysis

In Figs. 2 to 6, $n = 3$ replicates were used, where each replicate was an independent gel. Where error bars are shown, all values indicate the means ± SD. Significance was determined using a one-way analysis of variance (ANOVA) followed by Tukey's multiple comparison test in GraphPad Prism. In Fig. 7, $n = 4$ replicates were used for each group, where each replicate was a separate animal bearing a single injection. Significance was determined using a one-way ANOVA for each cytokine. In Fig. 8, $n = 4$ replicates were used for each group, where each replicate was a separate animal bearing two injections. Where error bars are shown, all values indicate the means ± SD. Significance was determined using a two-way repeated measures ANOVA followed by Sidak's multiple comparison test in GraphPad Prism.

Supplementary Materials

The PDF file includes:
Supplementary Text
Figs. S1 to S8
Table S1
Legends for movies S1 and S2

Other Supplementary Material for this manuscript includes the following:
Movies S1 and S2

REFERENCES AND NOTES

1. J. Thiele, Y. Ma, S. M. C. Bruekers, S. Ma, W. T. S. Huck, 25th anniversary article: Designer hydrogels for cell cultures: A materials selection guide. *Adv. Mater.* **26**, 125–148 (2014).
2. S. Correa, A. K. Grosskopf, H. Lopez Hernandez, D. Chan, A. C. Yu, L. M. Stapleton, E. A. Appel, Translational applications of hydrogels. *Chem. Rev.* **121**, 11385–11457 (2021).
3. R. Gharios, R. M. Francis, C. A. DeForest, Chemical and biological engineering strategies to make and modify next-generation hydrogel biomaterials. *Matter* **6**, 4195–4244 (2023).
4. N. Annabi, A. Tamayol, J. A. Uquillas, M. Akbari, L. E. Bertassoni, C. Cha, G. Camci-Unal, M. R. Dokmeci, N. A. Peppas, A. Khademhosseini, 25th anniversary article: Rational design and applications of hydrogels in regenerative medicine. *Adv. Mater.* **26**, 85–124 (2014).
5. C. Garcia Garcia, S. S. Patkar, B. Wang, R. Abouomar, K. L. Kiick, Recombinant protein-based injectable materials for biomedical applications. *Adv. Drug Deliv. Rev.* **193**, 114673 (2023).

Downloaded from https://www.science.org on September 06, 2025

6. A. M. Jonker, D. W. P. M. Löwik, J. C. M. van Hest, Peptide- and protein-based hydrogels. *Chem. Mater.* **24**, 759–773 (2012).
7. Y. Li, B. Xue, Y. Cao, 100th anniversary of macromolecular science viewpoint: Synthetic protein hydrogels. *ACS Macro Lett.* **9**, 512–524 (2020).
8. H. Li, N. Kong, B. Laver, J. Liu, Hydrogels constructed from engineered proteins. *Small* **12**, 973–987 (2016).
9. J. I. Bennett, M. O. Boit, N. E. Gregorio, F. Zhang, R. D. Kibler, J. W. Hoye, O. Prado, P. B. Rapp, C. E. Murry, K. R. Stevens, C. A. DeForest, Genetically encoded XTEN-based hydrogels with tunable viscoelasticity and biodegradability for injectable cell therapies. *Adv. Sci.* **11**, e2301708 (2024).
10. W. Zhang, A. W. Lohman, Y. Zhuravlova, X. Lu, M. D. Wiens, H. Hoi, S. Yaganoglu, M. A. Mohr, E. N. Kitova, J. S. Klassen, P. Pantazis, R. J. Thompson, R. E. Campbell, Optogenetic control with a photocleavable protein, PhoCl. *Nat. Methods* **14**, 391–394 (2017).
11. L. Li, J. M. Scheiger, P. A. Levkin, Design and applications of photoresponsive hydrogels. *Adv. Mater.* **31**, e1807333 (2019).
12. E. R. Ruskowitz, C. A. DeForest, Photoresponsive biomaterials for targeted drug delivery and 4D cell culture. *Nat. Rev. Mater.* **3**, 1–17 (2018).
13. J. A. Shadish, A. C. Strange, C. A. DeForest, Genetically encoded photocleavable linkers for patterned protein release from biomaterials. *J. Am. Chem. Soc.* **141**, 15619–15625 (2019).
14. D. Xiang, X. Wu, W. Cao, B. Xue, M. Qin, Y. Cao, W. Wang, Hydrogels with tunable mechanical properties based on photocleavable proteins. *Front. Chem.* **8**, 7 (2020).
15. R. Chapla, J. A. Hammer, J. L. West, Adding dynamic biomolecule signaling to hydrogel systems via tethered photolabile cell-adhesive proteins. *ACS Biomater. Sci. Eng.* **8**, 208–217 (2022).
16. J. Lei, H. Li, The photocleavable protein PhoCl-based dynamic hydrogels. *ACS Biomater. Sci. Eng.* **10**, 7404–7412 (2024).
17. X. Zhang, C. Dong, W. Huang, H. Wang, L. Wang, D. Ding, H. Zhou, J. Long, T. Wang, Z. Yang, Rational design of a photo-responsive UVR8-derived protein and a self-assembling peptide–protein conjugate for responsive hydrogel formation. *Nanoscale* **7**, 16666–16670 (2015).
18. S. Lyu, J. Fang, T. Duan, L. Fu, J. Liu, H. Li, Optically controlled reversible protein hydrogels based on photoswitchable fluorescent protein Dronpa. *Chem. Commun.* **53**, 13375–13378 (2017).
19. R. Wang, Z. Yang, J. Luo, I.-M. Hsing, F. Sun, B12-dependent photoresponsive protein hydrogels for controlled stem cell/protein release. *Proc. Natl. Acad. Sci. U.S.A.* **114**, 5912–5917 (2017).
20. Z. Yang, Y. Yang, M. Wang, T. Wang, H. K. F. Fok, B. Jiang, W. Xiao, S. Kou, Y. Guo, Y. Yan, X. Deng, W.-B. Zhang, F. Sun, Dynamically tunable, macroscopic molecular networks enabled by cellular synthesis of 4-arm star-like proteins. *Matter* **2**, 233–249 (2020).
21. B. Jiang, X. Liu, C. Yang, Z. Yang, J. Luo, S. Kou, K. Liu, F. Sun, Injectable, photoresponsive hydrogels for delivering neuroprotective proteins enabled by metal-directed protein assembly. *Sci. Adv.* **6**, eabc4824 (2020).
22. T. Duan, Q. Bian, H. Li, Light-responsive dynamic protein hydrogels based on LOVTRAP. *Langmuir* **37**, 10214–10222 (2021).
23. O. P. Narayan, X. Mu, O. Hasturk, D. L. Kaplan, Dynamically tunable light responsive silk-elastin-like proteins. *Acta Biomater.* **121**, 214–223 (2021).
24. Z. Yang, H. K. F. Fok, J. Luo, Y. Yang, R. Wang, X. Huang, F. Sun, B_{12}-induced reassembly of split photoreceptor protein enables photoresponsive hydrogels with tunable mechanics. *Sci. Adv.* **8**, eabm5482 (2022).
25. S. Chung, H. Lee, H.-S. Kim, M.-G. Kim, L. P. Lee, J. Y. Lee, Transdermal thiol–acrylate polyethylene glycol hydrogel synthesis using near infrared light. *Nanoscale* **8**, 14213–14221 (2016).
26. T. T. Lee, J. R. García, J. I. Paez, A. Singh, E. A. Phelps, S. Weis, Z. Shafiq, A. Shekaran, A. del Campo, A. J. García, Light-triggered in vivo activation of adhesive peptides regulates cell adhesion, inflammation and vascularization of biomaterials. *Nat. Mater.* **14**, 352–360 (2015).
27. R.-Z. Lin, Y.-C. Chen, R. Moreno-Luna, A. Khademhosseini, J. M. Melero-Martin, Transdermal regulation of vascular network bioengineering using a photopolymerizable methacrylated gelatin hydrogel. *Biomaterials* **34**, 6785–6796 (2013).
28. A. T. Hillel, S. Unterman, Z. Nahas, B. Reid, J. M. Coburn, J. Axelman, J. J. Chae, Q. Guo, R. Trow, A. Thomas, Z. Hou, S. Lichtsteiner, D. Sutton, C. Matheson, P. Walker, N. David, S. Mori, J. M. Taube, J. H. Elisseeff, Photoactivated composite biomaterial for soft tissue restoration in rodents and in humans. *Sci. Transl. Med.* **3**, 93ra67 (2011).
29. J. Elisseeff, K. Anseth, D. Sims, W. McIntosh, M. Randolph, R. Langer, Transdermal photopolymerization for minimally invasive implantation. *Proc. Natl. Acad. Sci. U.S.A.* **96**, 3104–3107 (1999).
30. W. Shen, K. Zhang, J. A. Kornfield, D. A. Tirrell, Tuning the erosion rate of artificial protein hydrogels through control of network topology. *Nat. Mater.* **5**, 153–158 (2006).
31. B. D. Olsen, J. A. Kornfield, D. A. Tirrell, Yielding behavior in injectable hydrogels from telechelic proteins. *Macromolecules* **43**, 9094–9099 (2010).
32. S. Roberts, T. S. Harmon, J. L. Schaal, V. Miao, K. J. Li, A. Hunt, Y. Wen, T. G. Oas, J. H. Collier, R. V. Pappu, A. Chilkoti, Injectable tissue integrating networks from recombinant polypeptides with tunable order. *Nat. Mater.* **17**, 1154–1163 (2018).
33. A. J. Olsen, P. Katyal, J. S. Haghpanah, M. B. Kubilius, R. Li, N. L. Schnabel, S. C. O'Neill, Y. Wang, M. Dai, N. Singh, R. S. Tu, J. K. Montclare, Protein engineered triblock polymers composed of two SADs: Enhanced mechanical properties and binding abilities. *Biomacromolecules* **19**, 1552–1561 (2018).
34. Y. Wang, P. Katyal, J. K. Montclare, Protein-engineered functional materials. *Adv. Healthc. Mater.* **8**, e1801374 (2019).
35. Y. Mizuguchi, Y. Mashimo, M. Mie, E. Kobatake, Temperature-responsive multifunctional protein hydrogels with elastin-like polypeptides for 3-D angiogenesis. *Biomacromolecules* **21**, 1126–1135 (2020).
36. P. Katyal, A. Hettinghouse, M. Meleties, S. Hasan, C. Chen, M. Cui, G. Sun, R. Menon, B. Lin, R. Regatte, J. K. Montclare, C. Liu, Injectable recombinant block polymer gel for sustained delivery of therapeutic protein in post traumatic osteoarthritis. *Biomaterials* **281**, 121370 (2022).
37. D. Britton, J. Legocki, D. Paul, O. Katsara, O. Aristizabal, N. Pandya, O. Mishkit, Y. Xiao, M. Aristizabal, N. Rahman, R. Schneider, Y. Z. Wadghiri, J. K. Montclare, Coiled-coil protein hydrogels engineered with minimized fiber diameters for sustained release of doxorubicin in triple-negative breast cancer. *ACS Biomater. Sci. Eng.* **10**, 3425–3437 (2024).
38. D. Britton, J. W. Sun, P. D. Renfrew, J. K. Montclare, Design of coiled-coil protein nanostructures for therapeutics and drug delivery. *Annu. Rev. Chem. Biomol. Eng.* **15**, 25–50 (2024).
39. P. B. Rapp, J. A. Baccile, R. P. Galimidi, J. Vielmetter, Engineering antigen-specific tolerance to an artificial protein hydrogel. *ACS Biomater. Sci. Eng.* **10**, 2188–2199 (2024).
40. X. Lu, Y. Wen, S. Zhang, W. Zhang, Y. Chen, Y. Shen, M. J. Lemieux, R. E. Campbell, Photocleavable proteins that undergo fast and efficient dissociation. *Chem. Sci.* **12**, 9658–9672 (2021).
41. V. Schellenberger, C. Wang, N. C. Geething, B. J. Spink, A. Campbell, W. To, M. D. Scholle, Y. Yin, Y. Yao, O. Bogin, J. L. Cleland, J. Silverman, W. P. C. Stemmer, A recombinant polypeptide extends the in vivo half-life of peptides and proteins in a tunable manner. *Nat. Biotechnol.* **27**, 1186–1190 (2009).
42. V. N. Podust, S. Balan, B.-C. Sim, M. P. Coyle, U. Ernst, R. T. Peters, V. Schellenberger, Extension of in vivo half-life of biologically active molecules by XTEN protein polymers. *J. Control. Release* **240**, 52–66 (2016).
43. P. Katyal, F. Mahmoudinobar, J. K. Montclare, Recent trends in peptide and protein-based hydrogels. *Curr. Opin. Struct. Biol.* **63**, 97–105 (2020).
44. F. Sun, W.-B. Zhang, A. Mahdavi, F. H. Arnold, D. A. Tirrell, Synthesis of bioactive protein hydrogels by genetically encoded SpyTag-SpyCatcher chemistry. *Proc. Natl. Acad. Sci. U.S.A.* **111**, 11269–11274 (2014).
45. D. Zhu, H. Wang, P. Trinh, S. C. Heilshorn, F. Yang, Elastin-like protein-hyaluronic acid (ELP-HA) hydrogels with decoupled mechanical and biochemical cues for cartilage regeneration. *Biomaterials* **127**, 132–140 (2017).
46. H. Wang, D. Zhu, A. Paul, L. Cai, A. Enejder, F. Yang, S. C. Heilshorn, Covalently adaptable elastin-like protein–hyaluronic acid (ELP–HA) hybrid hydrogels with secondary thermoresponsive crosslinking for injectable stem cell delivery. *Adv. Funct. Mater.* **27**, 1605609 (2017).
47. R. A. Suhar, M. S. Huang, R. S. Navarro, G. Aviles Rodriguez, S. C. Heilshorn, A library of elastin-like proteins with tunable matrix ligands for in vitro 3D neural cell culture. *Biomacromolecules* **24**, 5926–5939 (2023).
48. C. F. Guimarães, L. Gasperini, A. P. Marques, R. L. Reis, The stiffness of living tissues and its implications for tissue engineering. *Nat. Rev. Mater.* **5**, 351–370 (2020).
49. M. Kim, S. Tang, B. D. Olsen, Physics of engineered protein hydrogels. *J. Polym. Sci. B.* **51**, 587–601 (2013).
50. M. H. Chen, L. L. Wang, J. J. Chung, Y.-H. Kim, P. Atluri, J. A. Burdick, Methods to assess shear-thinning hydrogels for application as injectable biomaterials. *ACS Biomater. Sci. Eng.* **3**, 3146–3160 (2017).
51. M. Ju, K. Chen, B. Chang, H. Gu, UVA1 irradiation inhibits fibroblast proliferation and alleviates pathological changes of scleroderma in a mouse model. *J. Biomed. Res.* **26**, 135–142 (2012).
52. N. R. York, H. T. Jacobe, UVA1 phototherapy: A review of mechanism and therapeutic application. *Int. J. Dermatol.* **49**, 623–630 (2010).
53. K. Bedair, A. Elhadad, S. Hamad, J. Ferguson, P. Donnan, R. S. Dawe, No association between whole-body ultraviolet A1 phototherapy and skin cancers in humans: A cancer registry linkage study. *Br. J. Dermatol.* **183**, 586–587 (2020).
54. H.-W. Yeh, O. Karmach, A. Ji, D. Carter, M. M. Martins-Green, H. Ai, Red-shifted luciferase–luciferin pairs for enhanced bioluminescence imaging. *Nat. Methods* **14**, 971–974 (2017).
55. S. Zhang, H. Ai, A general strategy to red-shift green fluorescent protein-based biosensors. *Nat. Chem. Biol.* **16**, 1434–1439 (2020).

Downloaded from https://www.science.org on September 06, 2025

56. T. L. Rapp, C. A. DeForest, Visible light-responsive dynamic biomaterials: Going deeper and triggering more. *Adv. Healthc. Mater.* **9**, e1901553 (2020).
57. S. Pearson, J. Feng, A. del Campo, Lighting the path: Light delivery strategies to activate photoresponsive biomaterials in vivo. *Adv. Funct. Mater.* **31**, 2105989 (2021).
58. C. F. Guimarães, R. Ahmed, A. P. Marques, R. L. Reis, U. Demirci, Engineering hydrogel-based biomedical photonics: Design, fabrication, and applications. *Adv. Mater.* **33**, e2006582 (2021).
59. L. Xu, S. R. Gutbrod, A. P. Bonifas, Y. Su, M. S. Sulkin, N. Lu, H.-J. Chung, K.-I. Jang, Z. Liu, M. Ying, C. Lu, R. C. Webb, J.-S. Kim, J. I. Laughner, H. Cheng, Y. Liu, A. Ameen, J.-W. Jeong, G.-T. Kim, Y. Huang, I. R. Efimov, J. A. Rogers, 3D multifunctional integumentary membranes for spatiotemporal cardiac measurements and stimulation across the entire epicardium. *Nat. Commun.* **5**, 3329 (2014).
60. S. Wen, J. Zhou, K. Zheng, A. Bednarkiewicz, X. Liu, D. Jin, Advances in highly doped upconversion nanoparticles. *Nat. Commun.* **9**, 2415 (2018).
61. C. J. Bashor, I. B. Hilton, H. Bandukwala, D. M. Smith, O. Veiseh, Engineering the next generation of cell-based therapeutics. *Nat. Rev. Drug Discov.* **21**, 655–675 (2022).
62. R. Mout, R. C. Bretherton, J. Decarreau, S. Lee, N. Gregorio, N. I. Edman, M. Ahlrichs, Y. Hsia, D. D. Sahtoe, G. Ueda, A. Sharma, R. Schulman, C. A. DeForest, D. Baker, De novo design of modular protein hydrogels with programmable intra- and extracellular viscoelasticity. *Proc. Natl. Acad. Sci. U.S.A.* **121**, e2309457121 (2024).
63. N. K. Tripathi, A. Shrivastava, Recent developments in bioprocessing of recombinant proteins: Expression hosts and process development. *Front. Bioeng. Biotechnol.* **7**, 420 (2019).
64. M. A. Morris, R. A. Bataglioli, D. J. Mai, Y. Jung Yang, J. M. Paloni, C. E. Mills, Z. D. Schmitz, E. A. Ding, A. C. Huske, B. D. Olsen, Democratizing the rapid screening of protein expression for materials development. *Mol. Syst. Des. Eng.* **8**, 227–239 (2023).

Acknowledgments: We would like to acknowledge D. Whittington for training and maintenance of the UW Mass Spectrometry Center. We also acknowledge helpful advice, feedback, and training from T. Rapp, I. Kopyeva, R. Bretherton, M. O'Kelly Boit, J. Bennett, and R. Francis. **Funding:** This work was supported by the National Science Foundation Graduate Research Fellowship Program DGE-2140004 (N.E.G., O.P., and A.F.), NIH Maximizing Investigators' Research Award R35GM138036 (C.A.D.), NIH R01DK128551 (K.R.S.), NIH U01CA281848 (J.M.O.), Wellcome Leap as part of the HOPE program (K.R.S.), W. M. Keck Foundation (K.R.S.), Allen Distinguished Investigator Award (K.R.S.), and Paul G. Allen Frontiers Group advised grant of the Paul G. Allen Family Foundation (K.R.S.). Part of this work was conducted with instrumentation provided by the Joint Center for Deployment and Research in Earth Abundant Materials (JCDREAM), and H&E and IHC analysis was supported by the Experimental Histopathology Shared Resource, RRID:SCR_022612 (https://scicrunch.org/resolver/RRID:SCR_022612), of the Fred Hutch/University of Washington/Seattle Children's Cancer Consortium (P30 CA015704, supporting the Fred Hutch Histopathology core). **Author contributions:** Conceptualization: C.A.D. and N.E.G. Methodology: N.E.G., F.Z., Y.S., and L.A. Investigation and analysis: N.E.G., F.Z., Y.S., L.A., O.P., A.F., and K.R.S. Resources: C.A.D., K.R.S., and J.M.O. Visualization: N.E.G. Supervision: C.A.D. Writing—original draft: C.A.D. and N.E.G. Writing—review and editing: C.A.D., N.E.G., and Y.S. **Competing interests:** The authors declare that they have no competing interests. **Data and materials availability:** All data needed to evaluate the conclusions in the paper are present in the paper and/or the Supplementary Materials.

Submitted 10 March 2025
Accepted 29 July 2025
Published 27 August 2025
10.1126/sciadv.adx3472

Downloaded from https://www.science.org on September 06, 2025